Influence of Halogen Substituents on the Photophysical Properties of 7-Hydroxycoumarin: Insights from Experimental and Theoretical Studies

Bryson A. Hawkins,[1,6*] Liam D. Adair,[4,5] William G. Ryder,[4] Jonathan J. Du,[1] Elias Najib,[1] Elizabeth J. New,[4,5] Philip A. Gale,[2,4] James A. Platts,[3] Paul W. Groundwater,[1] and David E. Hibbs.[1]

[1]*Sydney Pharmacy School, Faculty of Medicine and Health, The University of Sydney, NSW 2006 Australia*

[2] *Faculty of Science, University of Technology Sydney, City Campus, Broadway, NSW 2007 Australia*

[3]*School of Chemistry, Cardiff University, Cardiff, CF10 3AT, UK*

[4] *School of Chemistry, Faculty of Science, The University of Sydney, NSW 2006 Australia*

[5] *Australian Research Council Centre of Excellence for Innovations in Peptide and Protein Science, The University of Sydney, NSW 2006 Australia*

[6] *Current Address: Antimicrobial Discovery Centre, College of Science, Northeastern University, Boston, 02115 MA, USA*

**Corresponding author: Bryson A. Hawkins, bryson.hawkins@sydney.edu.au*

†Electronic supplementary information (ES) available. CCDC: 2376831, 2376829 and 2376830 *for (**1**), (**2**) and (**3**) For ESI and crystallographic data in CIF or other electronic formats, see DOI: XXXXXXX*

Abstract

The benzopyrone molecule coumarin is a popular fluorescent scaffold, but how chemical modifications affect its properties is not well understood. We investigated this using halogenated 7-hydroxycoumarin, unsubstituted 4-methylumbiliferone, and ortho-chloro and bromo substitutions on the phenolic ring. Charge density data from X-Ray diffraction and computational methods revealed that halogenation at the ortho position significantly reduced quantum yield (QY). Specifically, 7-hydroxycoumarin (**1**) had a QY of 70%, while ortho-chloro (**2**) and ortho-bromo (**3**) had QYs of 61% and 30%, respectively. Experimental data showed that these molecules excited similarly, but the electrostatic potential and dipole moments indicated that **2** and **3** dissipated excitation energy more easily due to charge separation. The heavy-atom effect of Cl and Br did not fully explain the QY reductions, suggesting other radiative decay processes were involved. By incorporating spin-orbit coupling (SOC) effects, we estimated intersystem crossing (ISC) and phosphorescence rates, providing theoretical QYs of 78% for **1**, 59% for **2**, and 15% for **3**. The large deviation for **3** was attributed to its higher SOC potential derived in computational calculations. Our overall findings indicate that **3**'s reduced QY results from a mix of SOC-induced ISC and charge dissipation due to the electronegative of Br atom, while **2**'s reduction is primarily due to charge separation caused by Cl alone. Further studies are needed to validate this approach with other scaffolds.

Introduction

Fluorescence is the ability for a molecule to emit light after being excited by an incoming photon. Research in fluorescence control is ever-growing, where tailored molecules (probes)

may be used as signals for many chemical and biological processes.[1-6] These processes include ion movement across membranes, chemical reactions, and bacterium detection.[7-10] Although, much research has been conducted in this area, there is ambiguity in understanding how the sensitivity and specificity of a fluorophore changes upon chemical substitution.[11] Previous studies have found that certain substitutions in appended groups had unpredictable trends on the probe's sensitivity or specificity.[5, 12-15] These variations take form as changes in intensity, emission wavelength, lifetime or quantum yield (QY) which occur to the electron density between ground and excited states.[9] An example of appended groups is halogenated probes that are known to quench better then amines, but have larger level of tunability based on p*K*a.[16] Although, at the same time it is seen that within a series of probes fluorescence variations are created by the appendage position, number and type of halogens, which complicates their use.[17] Considering other branches of medicinal chemistry, there are tools for drug design and crystal engineering[18], leading to the question: Is there a way to rationally design and tailor the photophysical behavior of fluorophores?

From the governing principles of Franck-Condon (FC) and Herzberg-Teller (HT) factors fluorescence can be related to a molecule's valence electron excitation behavior in response to photon excitation.[8, 19] This means that examining the ground-state electron density distribution (EDD) using charge density combined with density functional theory (DFT) may allow a path to probe design.[10, 20-33] Previously, we used crystalline geometries to explain excited-state charge movement in a fluorophore by an external modulator, imidazole, with density functional theory (DFT).[34] In this manuscript, we explore internal appendage changes on a methylumbelliferone series (Scheme 1). Using photoluminescence studies, high-resolution charge density single crystal X-Ray diffraction and DFT calculations the effects of halogenation of the phenolic ring on QY is explored. It is hoped that these results

simulate rational design of probes by exploring the EDD movement between electronic states.

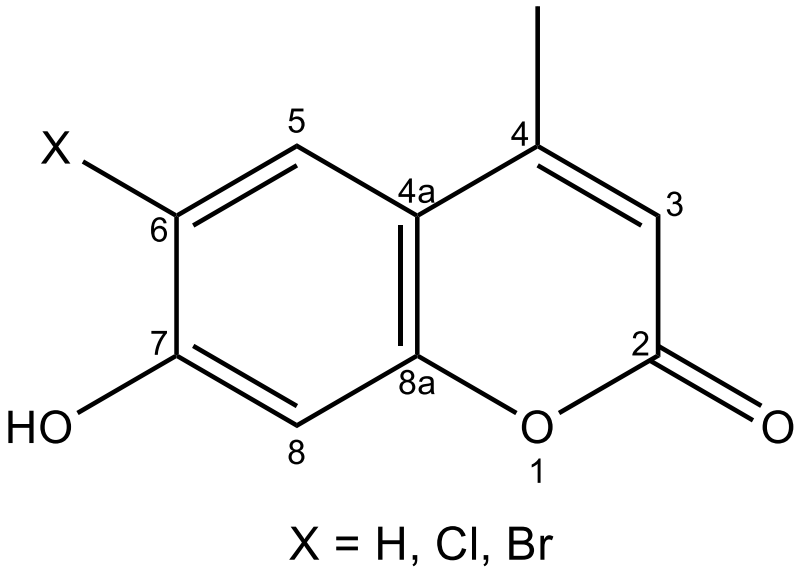

Scheme 1: Molecular representation of Substituted4-methyl umbelliferone, where X is the 6th position. **1**, X=H, **2** X=Cl and **3**, X=Br.

Methods

Synthesis

For compounds **2** and **3**, halogenation of the, 6 position (Scheme 1) was achieved using Pechmann condensation reactions of 4-chlororesorcinol and 4-bromoresorcionol, respectively. The reaction of halogenated resorcinol with ethyl acetoacetate was performed using the method of Kinoshita *et al.*[5] The products were characterized by single-crystal X-Ray diffraction, and nuclear magnetic resonance, infrared spectroscopy, and mass spectrometry (ESI, Figure S3 and S4).

Photophysical studies

The luminescence of UV absorption, fluorescence excitation and emission, lifetimes, and relative QYs were obtained for **1**, **2**, and **3**. Full experimental methods for gaining the photochemical results can be found in ESI, (Figure S5 – 7). The collections for the relative QY were obtained using the integrated emission spectra which was then plotted against the absorbance at 320 nm. The QY yield of 4-methylumbelliferone **1** is reported as 0.70.[35] The relative quantum yields of **2** and **3** were calculated using the following formula:

$$\boldsymbol{\Phi_s} = \boldsymbol{\Phi_r}\left(\frac{\boldsymbol{m_s}}{\boldsymbol{m_r}}\right)^2 \qquad (1)$$

$\boldsymbol{\Phi}$ = Quantum yield

m = gradient of the plot of integrated fluorescence intensity against absorbance

r = reference

s = sample

Single Crystal Growth

Single crystals of **1**, **2** and **3** were grown *via* slow evaporation from a dichloromethane (DCM) solution. For all crystals, the samples were dissolved in excess DCM and then left to slowly evaporate covered with a single piece of parafilm. Crystals suitable for diffraction were formed within 1 week.

X-Ray Diffraction data collection, data treatment, and refinement.

The high-resolution X-Ray diffraction experiments were performed as follows. All single crystals were selected by hand using an Olympus SZ61 rotating stage microscope. The diffractions of **1**, **2** and **3** were collected on a Rigaku SuperNova™ Dual Source System at MoKα (λ = 0.71073) with a CCD Atlas detector. Full diffraction experimental details including refinement techniques can be found in ESI. The topology of the crystalline ground states EDD was performed using XDPROP, within XD-2016.[36] The topological analysis of all densities satisfied the Morse equation.[37]

Computational methods

Various computational methods employed in throughout this study will be described below according to application. All calculations were performed using ORCA 5.0.3.[38]

Validation of the experimental EDD.

To ensure the accuracy of the experimental ground-state EDD obtained *via* the multipole models (MMs); each compounds' MM was compared to the EDD derived from a DFT wavefunction. The wavefunctions were obtained using the high-order cartesian coordinates (sin θ/λ>0.8) with all covalent hydrogen bonds (X-H) fixed at neutron lengths as an input geometry for single-point (SP) calculations. The calculations were performed using the coulombic-attenuating long-range hybrid exchange functional (CAM-B3LYP) and the DEF2-TZVP basis set.[38-42] This functional and basis set combination was selected due to is balance of accuracy and speed in both ground and excited state calculations that was scalable with increasing system complexity. The resultant molecular graphs were calculated with AIMALL,[43] All of which satisfied the Poincaré–Hopf theorem.[44] The DFT topologies were in good agreement with the experimental EDDs gained from X-Ray diffraction. The largest variation in the EDD between DFT and the experimental EDDs was seen in **1** (ρ = 0.18 (eÅ^{-3})

and for $\nabla^2\rho$ = -8.05 ($e\text{Å}^{-5}$), the raw data for these comparsion can be found in ESI (Table S13-21.)

Theoretical Generation of Fluorescence Spectra.

Theoretical fluorescence spectra of **1**, **2** and **3** were obtained following the methods of De Souza *et al*.[45] The same input geometries from SP calculations were used for optimization and frequency calculations of the ground state (S_0) in an equilibrium based conductor-like continuum model (LR-CPCM) solvent systems of water using restricted Kohn-Sham DFT. Then, the S_0 optimized geometries were used at the input for determination of the optimized first-excited state (S_1). Similarly, this used the LR-CPCM water, however, time-dependent (TD)-DFT was used with 30 roots, no mixing of singlet or triplet MOs at CAM-B3LYP / DEF2-TZVP theory.[46, 47] The spectra are then obtained using the excited state dynamic (ESD) module in ORCA, which applies fermi's golden rule within the path integral approach to analysis the normal mode displacement between energetic states.[45]

Theoretical Calculation of Spin-Orbital Coupling.

The spin-orbit coupling (SOC) potential of **1, 2** and **3** were obtained using TD-DFT. Using the S_0 optimized geometry was the initial state in TD-DFT calculations. The calculations had spin-orbit coupling enabled and used the relativistic correction (ZORA). All calculations were performed CAM-B3LYP/ ZORA-DEF2-TZVP with solvation controlled by LR-CPCM water generating 30 roots.[46-48] To further check the spin orbit coupling changes moving from non-halogenated to halogenated down the group, the halogen on the fluorophore was replaced with both fluorine and iodine.[49] The structures were optimized in the same manner as generation of S_0, above, prior to spin-orbit calculations. This can be seen in ESI Figure S8.

Intersystem crossing predictions and Estimated QY.

The intersystem crossing (ISC) can be estimated using the ESD module in ORCA.[38] Here, the path integral approach used for fluorescence calculations is expanded to follow the normal mode frequencies between the singlet S_x and triplet, T_x states.[38] The triplets states were determined by reviewing the TD-DFT output for the mixing MOs.[50] The SOC matrices for each compound showed the mixing MOs were the first three triplet states.[50] Each triplet state was optimized in the same manner as the S_x states (CAM-B3LYP/ DEF2-TZVP). Then the degree of intersystem crossing was calculated by summation of the rate constant k_{isc} for all T_x. This is represented in the summation equation (5). Lastly, the density in the triplet state needs to be calculated, this can be performed using a path integral approach, where the rate is the average over the triplet sublevels as represented in Equation 6.[9, 51]

$$k_{isc}(obs) = \sum_{Triplet\ Lower}^{Triplet\ Upper} k_{isc}(T^1) + k_{isc}(T^{-1}) + k_{isc}(T^0) \qquad (2)$$

$$k_{phosphor}(obs) = \frac{k_1 + k_{-1} + k_0}{3} \qquad (3)$$

Using the rates derived from Equations 2 and 3 the theoretical Quantum Yield of fluorescence, Φ_{TE}, can estimated by the percentage sum of rates k_x and it is represented in equation 4, where, k_f, k_{isc}, $k_{phosphor}$ are the rates of fluorescence, intersystem crossing and phosphorescence respectively.

$$\Phi_{TE} = \frac{k_f}{k_f + k_{isc} + k_{phosphor}} \times 100 \qquad (4)$$

Results and Discussion

The photophysical properties of **1**, **2** and **3**, followed previous reports of R-group changes created by halogens on coumarin based scaffolds.[52] Figure 1 shows the experimental fluorescence spectra of **1**, **2** and **3**. Here, it is shown that across all pH environments the excitation and emission regions for each probe is similar, as summarized in Table 1. Figure 1 indicates that **1** is significantly more fluorescent than both halogenated derivatives **2** and **3**. It is also evident that in water the fluorophores are in a protonation equilibrium at pH 7. In basic solutions, the fluorophores would be deprotonated at the 7-hydroxy position based on the pKa of the phenol being ~10.[53] This has the most intense effect on the absorption of **1**, with a 3-fold increase in intensity compared to **2** and **3**. These results are not unprecedented, with the emission profile changing from FC to HT emission.[34] Similar to the Hawkins *et al.* finding for 2-methylimidozole acting as an electron withdrawing agent. For **2** and **3** the -Cl and -Br are destabilizing the phenolic rings towards vibronic emission slightly but are not strong enough electron withdrawing agents to swap the emission profile as shown in water *vs*. NaOH environment. This is highlighted in Figure 1(b) because if the halogen's electron withdrawing potential was the culprit, **2** would be the least fluorescent but the change in intensity is minor when exposed to a basic environment. As such, the R-group change have an alternative manner for decreasing the fluorescence emission. To understand this loss, fluorescence lifetimes and experimental QY's were obtained. The summarized photophysical properties, including fluorescence lifetimes and relative QYs are in Table 1.

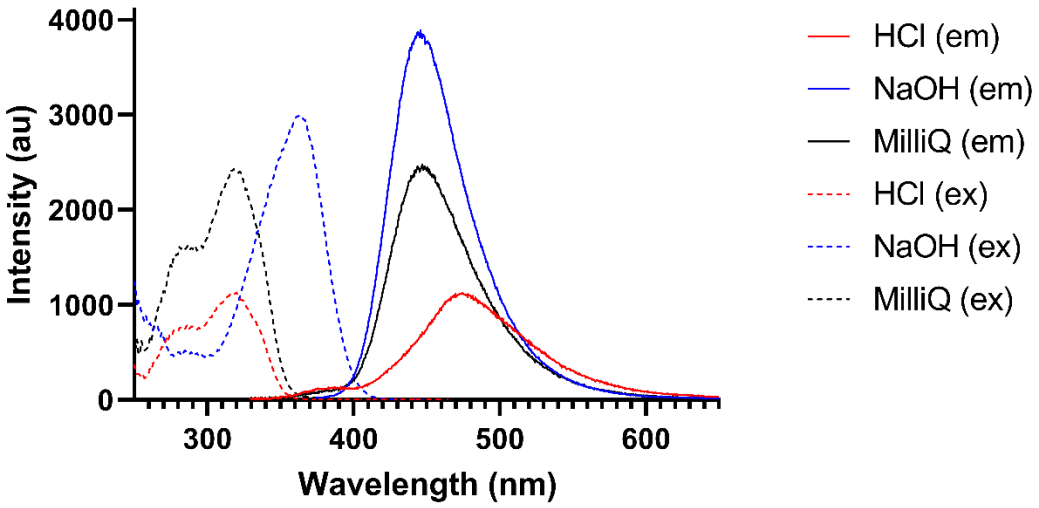
4000
3000
2000
1000
0
Intensity (au)
300
400
500
600
Wavelength (nm)
HCl (em)
NaOH (em)
MilliQ (em)
HCl (ex)
NaOH (ex)
MilliQ (ex)

(a)

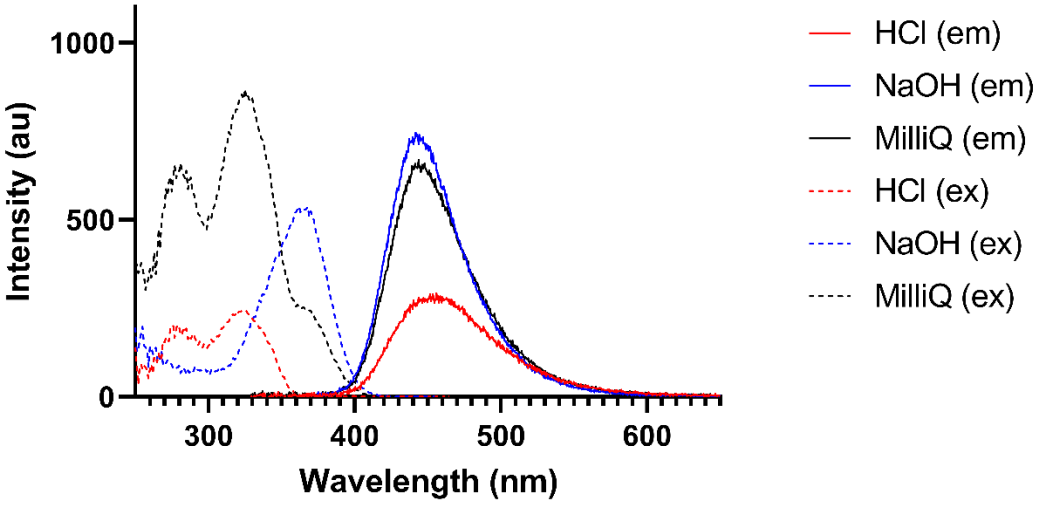
1000
500
0
Intensity (au)
300
400
500
600
Wavelength (nm)
HCl (em)
NaOH (em)
MilliQ (em)
HCl (ex)
NaOH (ex)
MilliQ (ex)

(b)

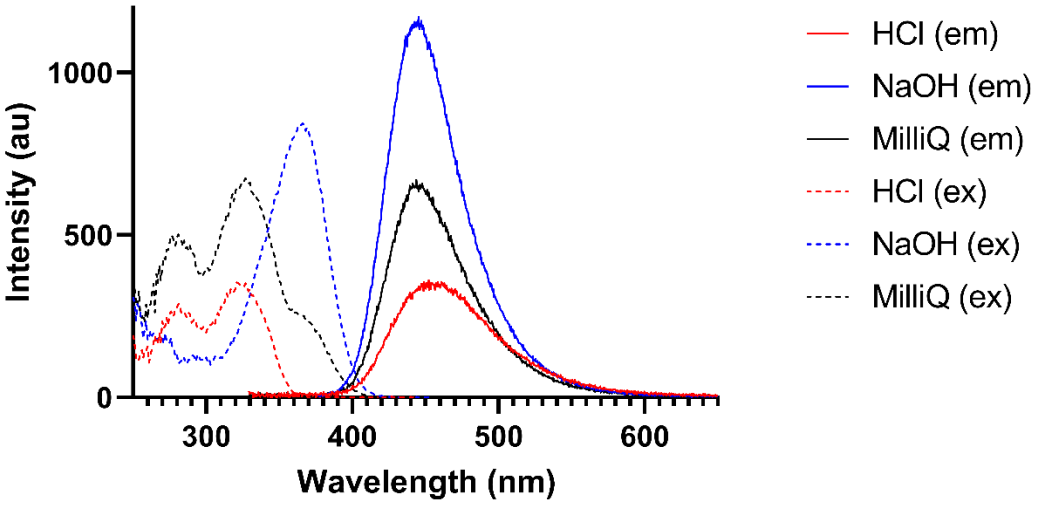
1000
500
0
Intensity (au)
300
400
500
600
Wavelength (nm)
HCl (em)
NaOH (em)
MilliQ (em)
HCl (ex)
NaOH (ex)
MilliQ (ex)

(c)

Figure 1: The experimental excitation and emission spectra of **1**, **2** and **3**, a, b, and c respectively in various pH-controlled solvents, HCl pH=2, and NaOH pH=10.

Table 1: Summary of photophysical properties in H_2O:

compound	λ_{abs} (nm)	λ_{ex}(nm)	λ_{em}(nm)	τ /lifetimes (ns)	Φ
1	321	318	447	6.00	0.70[35]
2	326	325	444	4.70	0.61
3	326	327	444	3.61	0.31

Table 1, shows halogen substitution leads to a decreased fluorescence lifetime and QY in **2** and **3**. The loss of lifetime and QY can result from a number of factors. One possibility is insufficient absorption, but this is ruled out by the absorption spectra of each compound be near identical (ESI, Figure S6). Another option is that the excitation can be lost by collision / energy dissipation within the system (solvents, molecules, *etc*), or formally forbidden spin-orbit interactions.[9] This can be reviewed experimentally when considering the static ground state EDD of the system using the experimental charge density, below.

Crystallography

Previous applications of charge density single crystal X-ray diffraction have been able to link static experimental ground state EDD to dynamic real-world properties such as stability and solubility.[10, 22, 33, 34, 54-56] We therefore performed crystallographic analysis of **1**, **2** and **3**, looking for EDD artefacts that may correlate fluorescence changes. Table 2 shows has selected crystallographic data of the systems, whilst Figure 2 depicts the independent atomic models (IAMs). The discussed geometry and topology of the EDD systems were

reviewed to ensure accuracy before looking at aromatic localisation properties, this can be found in ESI.

Table 2: Selected crystallographic Data.

Compounds	**1**	**2**	**3**
Formula	$C_{10}H_8O_3 \cdot H_2O$	$C_{10}H_7O_3Cl_1$	$C_{10}H_7O_3Br_1$
Molecular Mass (g/mol)	194.18	210.61	255.06
Crystal size (mm)	0.2 x 0.3 x 0.3	0.4 x 0.3 x 0.3	0.4 x 0.3 x 0.2
Temperature (K)	150 (0)	150 (2)	150 (0)
Wavelength (Å)	MoKα (λ = 0.71073)	MoKα (λ = 0.71073),	MoKα (λ = 0.71073)
Crystal system	Monoclinic	Monoclinic	Monoclinic
Space group	$P2_1/n$	$P2_1/n$	$P2_1/n$
a (Å)	6.97657(18)	7.3534 (1)	7.5046 (1)
b (Å)	11.3024(2)	10.1633 (1)	10.2993 (2)
c (Å)	11.7801(2)	11.7576(1)	11.6853 (2)
β°	105.577(3)	99.018 (1)	99.252 (2)
Volume ($Å^3$)	105.576(2)	867.841(17)	891.43 (2)
Z	4	4	4
Refinement Method	full-matrix least squared refinement on F^2	full-matrix least squared refinement on F^2	full-matrix least squared refinement on F^2
No. unique	7441	7192	7452
R_{int}	0.047	0.049	0.036
Completeness (%)	99.40	98.93	99.9
No. reflections used	7276	7192	7464
ρ_c (g cm^{-1})	1.44	1.612	1.915
F(000)	408	432	508
μ (mm^{-1})	0.112	0.412	4.574
R(*F*), *R*(F^2), all data	0.0565, 0.1604	0.0347, 0.089	0.0238, 0.0600

Goodness of fit	1.032	1.087	1.021
Residual density (e Å^{-3})	-0.26, 0.53	-0.20, 0.68	-0.58, 0.85
Multipole Model (TDS)			
sin θ/λ	1.00	1.110	0.999
$R(F)$, $R(F^2)$, all data	0.0546, 0.0972	0.0623, 0.0933	0.0187, 0.0225
Residual density (e Å^{-3})	-0.413, 0.422	-0.293, 0.282	-0328, 0.317
Nvar/Nref	15.55	25.49	19.30

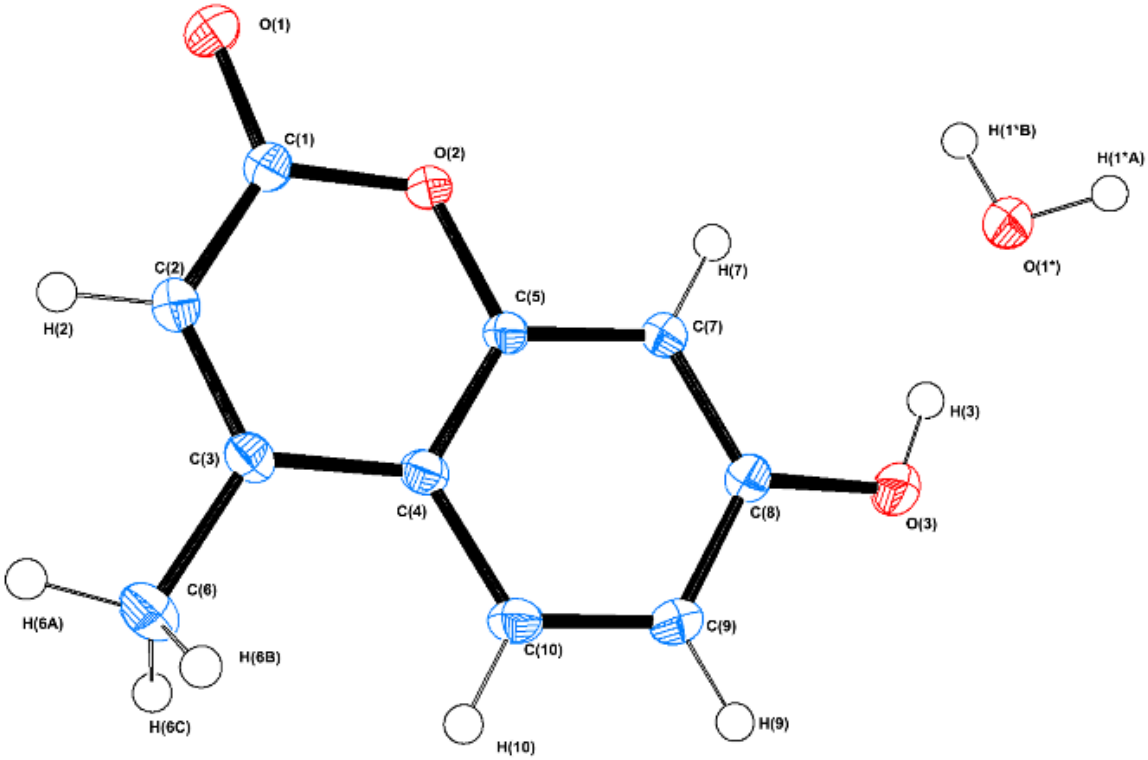

(a)

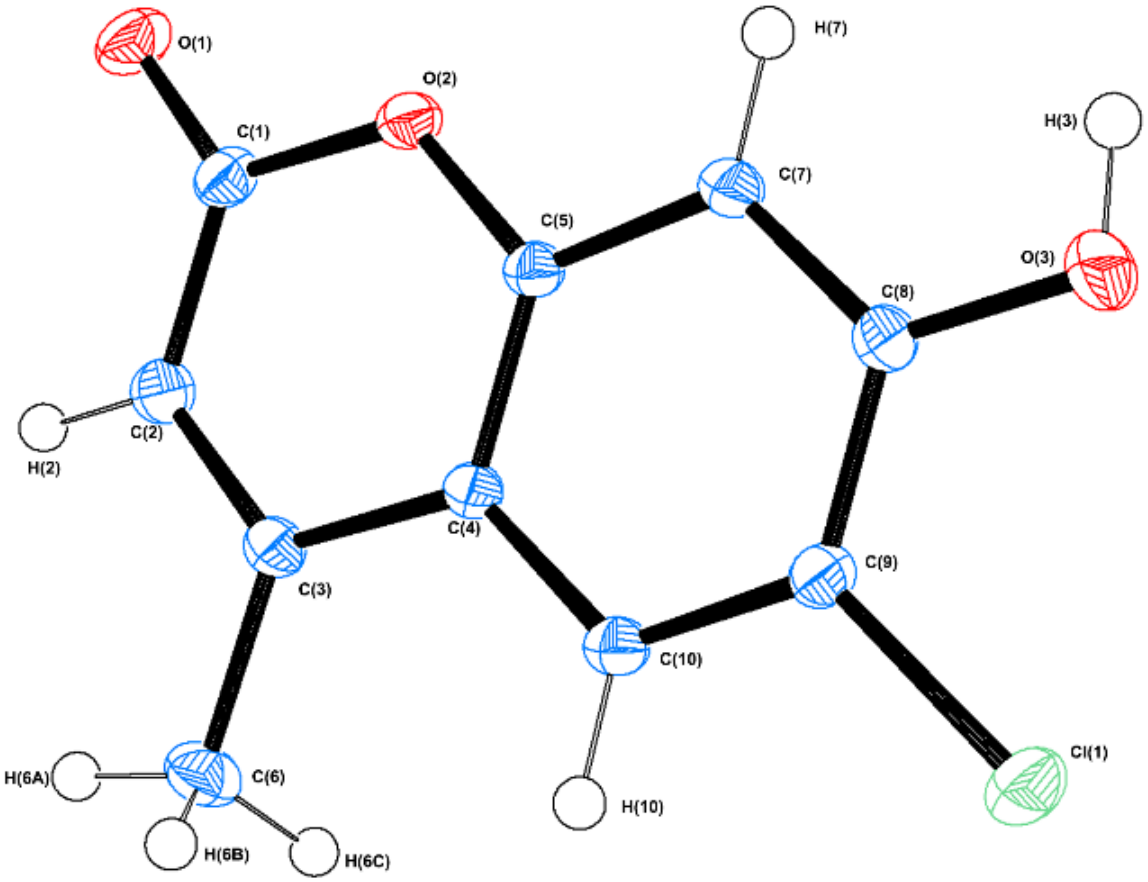

(b)

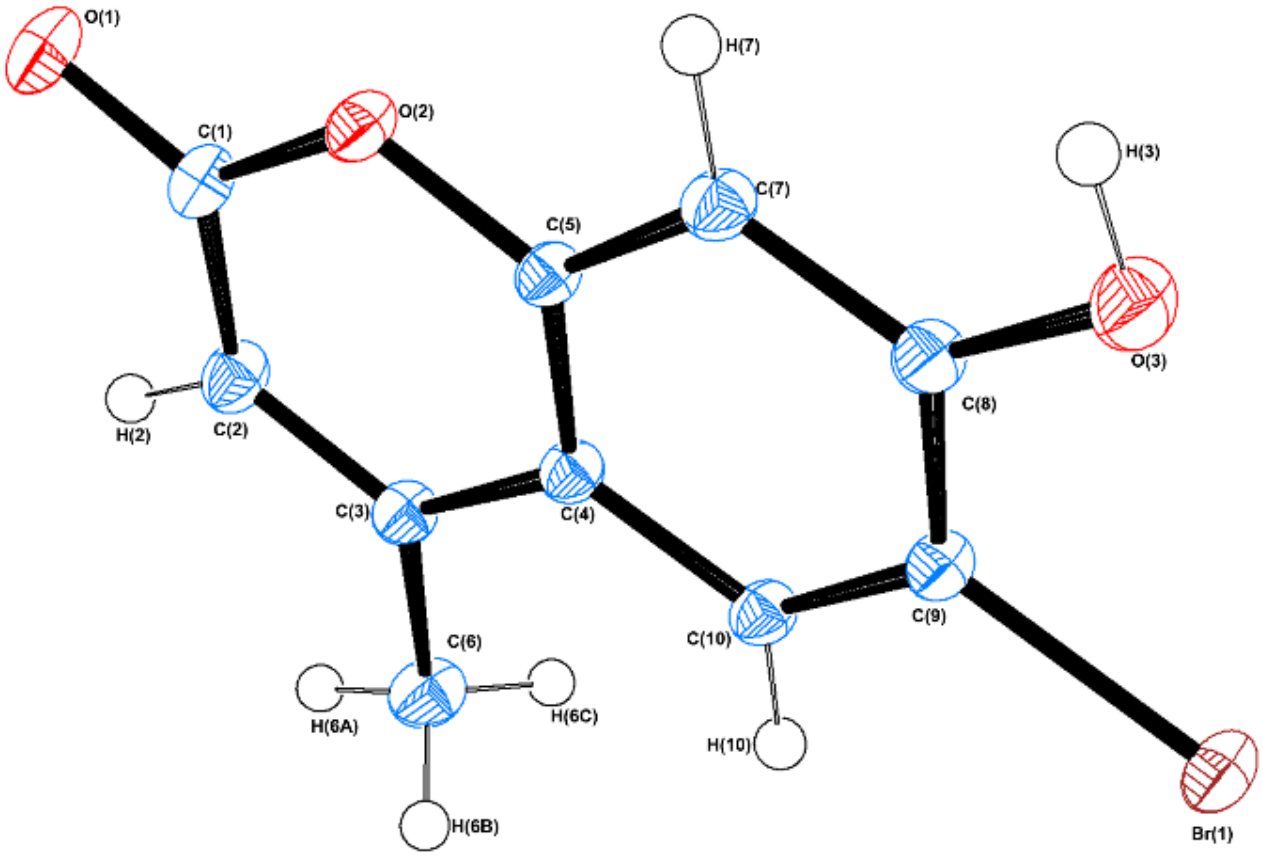

(c)

Figure 2: (a),(b), and (c). Oak-Ridge Thermal ellipsoid plots of **1**, **2** and **3**, respectively, plotted at 50% probability.

Applications of crystallography to explain fluorescence profiles is uncommon, [34] however, it has been shown that electrostatic potential (ESP) and frontier orbitals are related to the chemical reactivity and regioselectivity of photoproducts.[57, 58] Frontier orbitals cannot be derived from the experimental EDD, although there is a continual drive to develop a robust orbital-free model.[58-60] From the luminescence results above 1, 2 and 3 excite equally, this should be evident in the EDD electrostatics, ESP. This is because ESP directly quantifies the static charge separation across the molecule.[44] In the past, where the electrostatics are unequally distributed in the excitation of S_0 to S_1 caused an increased demand for energetic

relocation/redistribution to re-equilibrate the EDD.[61] This can occur by using hydrogen bonding, and also when an electron-hole systems forms to dissipate the photons energetic effect.[62 63]. Figures 3 a-c show isosurfaces of ESP plotted along a ρ isosurface scaffold, these plots were generated using CrystalExplorer centred around C(4) as an origin with boundaries to encapsulate the entire asymmetric unit.

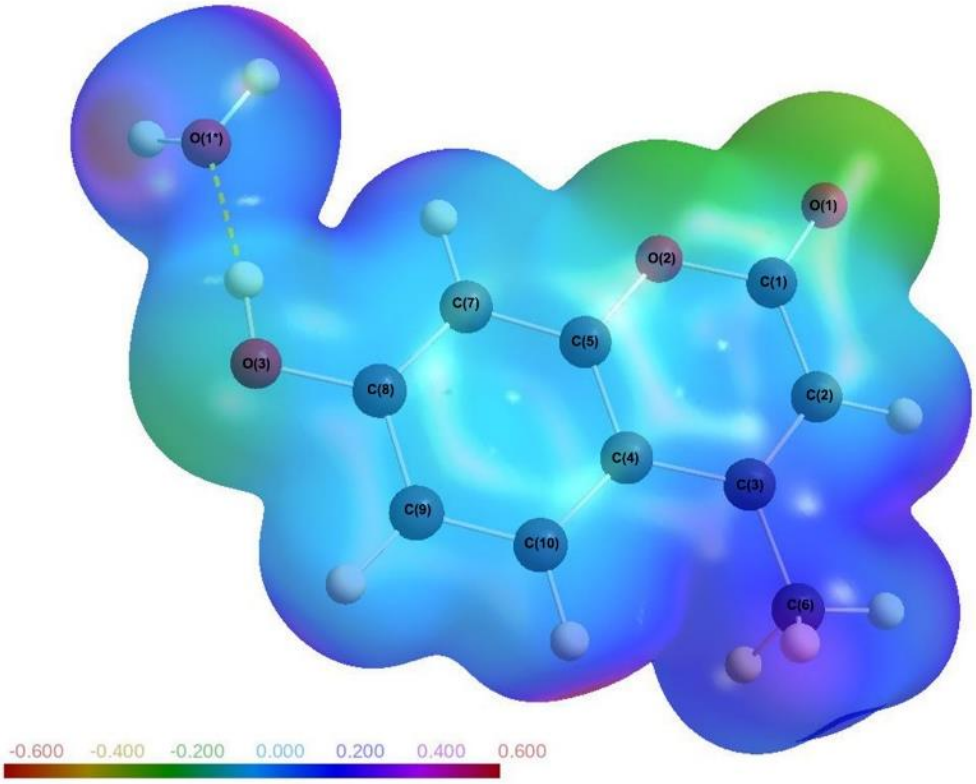

(a)

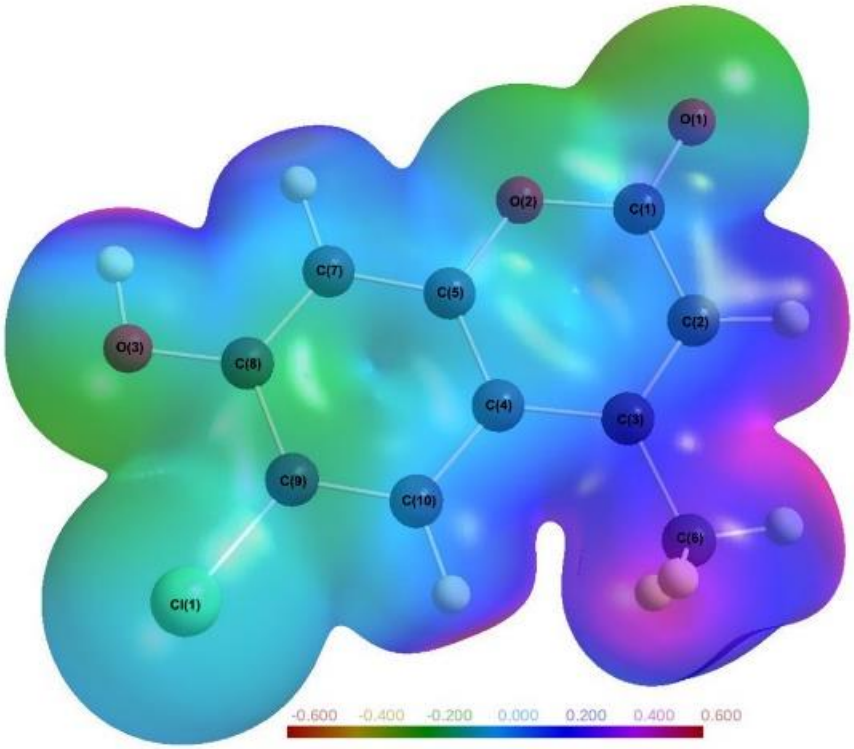

(b)

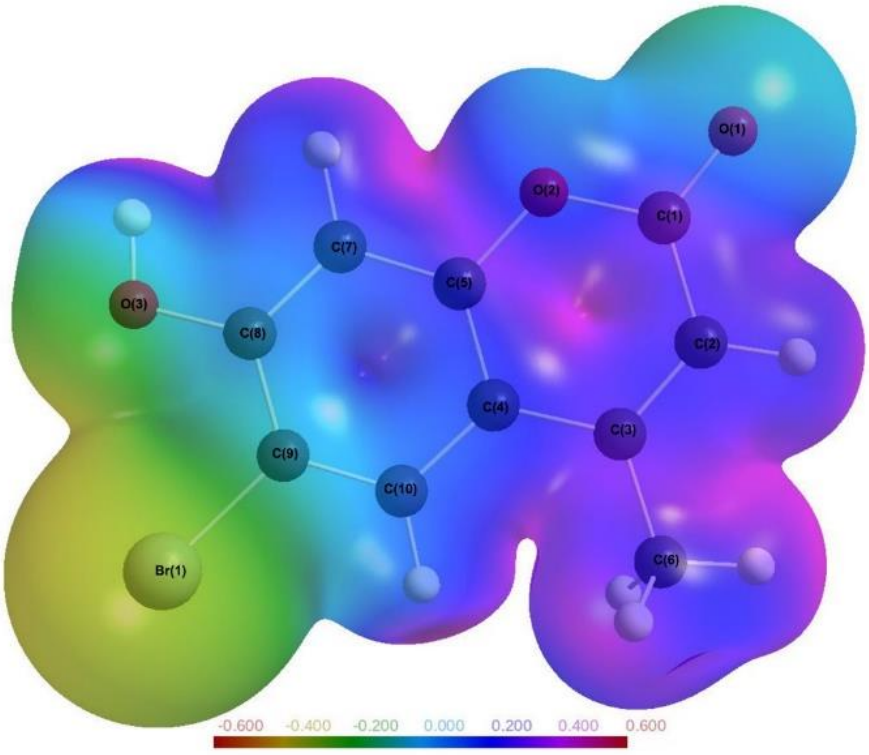

(c)

Figure 3: Molecular electrostatic potential maps of **1**, **2** and **3** (a),(b) and (c), respectively. Electrostatic potential mapped on an isosurface of ρ. Plots generated at +/- 0.5e isoelectronic density.

Figure 3a, shows the hydrate co-crystal does not have much of an impact on the ESP neutrality along the surface. Further to this, a similar trend is seen in Figure 3b **2**, where, although the chlorinated phenolic ring does cause an increase in electronegative character it does not create a significant level of charge separation along the ring. This is compared to Figure 3c, **3**, where the bromination of the phenolic moiety has an increased level of electrostatic pull toward the Br atom in **3**, with the lactone fragment being slightly more electropositive compared to **1** and **2**. The gradient of ESP in **3** around the Br atom indicates a significant positive gap between C(9)-Br(1), this increased charge change can be linked to the formation of larger σ-holes that are vital for bonding outside of the asymmetric unit, which vital for the formation of homosynthon for **3**.[63] Previously, in a graphene derivative a larger degree of electronegativity gave rise to fluorescence modification *via* ISC upon halogenation of the probe[64] These ESP findings indicate that Br causes **3** to have larger negative ESP point adjacent to the aromatic system creating a stronger homosynthon system than **2**. These Columbic bonds have been seen to create an energy-exchange potential previously.[65] This potential allows the C-halogen intramolecular bond to equilibrate the EDD and photochemical properties of the molecule.[66] This coincides with the spectroscopic results that each system should excite equally, but, for further validation, the aromatic character of these systems is to compare the ring critical point densities in **2** and **3** may highlight variations in the localization of the EDD. For the halogenated rings, there is a 0.03 e Å^{-3} increase in ρ for the brominated fluorophore (0.046 v. 0.076 e Å^{-3}, **2** and **3** respectively). This density is moved from the lactone fragment towards the Br atom reflecting the ESP plots above. This movement creates and inequality in the $\nabla^2\rho$ which decreases in **3** by 1.8 e Å^{-5} (6.0 v. 4.2 e Å^{-5}, for the lactone ring for **2** and **3** respectively). This suggests there is a shift in the valence charge of the aromatic rings for **3**. To review this, we

applied the HOMA index (Harmonic Oscillator Model of Aromaticity) was used. A HOMA measure between 0-1 that grades whether a molecule is completely aromatic, 1, or non-aromatic, 0.. The HOMA can be derived using the following expression, equation (5).

$$HOMA = 1 - \frac{\alpha}{n}\sum_{i=1}^{n}(R_i - R_{opt})^2 \quad (5).$$

In the expression, n is the number of atoms in the ring system, α is a constant for the system make-up, R_i and R_{opt} are the bond lengths from experimental data and optimised systems, respectively. The values for α and R_{opt}, were taken from the reference text of Krygowski *et al*.[67] The derived HOMA index for **1**, **2** and **3** can be found in Table 3, the experimental and comparison of S_0 and S_1 optimised geometries are present to draw a comparison.

Table 3: HOMA indexes for **1**, **2** and **3**.

Compound	EXP, S_0 and S_1	Lactone Ring (C(1)-C(2)-C(3)-C(4)-C(5)-O(2)-)	Phenolic/Halogenation Ring (C(4)-C(10)-C(9)-C(8)-C(7)-C(5)-)
1	EXP	0.95	0.94
1	S_0	0.90	0.89
1	S_1	0.49	0.41
1 Water removed	S_0	0.90	0.92
1 Water removed	S_1	0.65	0.69
2	EXP	0.94	0.94
2	S_0	0.91	0.92
2	S_1	0.50	0.40
3	EXP	0.88	0.93
3	S_0	0.87	0.92

3	S_1	0.52	0.39

Table 3 shows all compounds in the EXP or S_0 have a high HOMA score, indicating each molecule is in an aromatic state. However, upon excitation, π^* state, each molecule becomes anti-aromatic and then re-establishes the S_0 EDD equilibrium. It is seen that the hydrate form of **1** in the $S_{0/1}$ is not a perfect comparison for HOMA compared to **2** and **3**. This can be simply attributed to the hydrate molecule in π^* displaces the energy into the hydrogen bonding network, attenuating the anti-aromatic state. In the HOMA analysis for **2** and **3** there is degree of aromaticity is near equal in all theoretical optimised structures. Although, in the EXP data the brominated form **3** is slightly less aromatic in the ground-state. Looking closer at the reactivity of these charge surfaces using the crystalline dipole moment for **2** and **3** there is a large degree charge separation compared **1**. The dipole moments are 5.96, 12.58 and 18.96 D for **1**, **2** and **3**, respectively. This correlates with the ESP plots, where the ESP can be visual seen to shift towards the halogen atoms, this is also known to give rise to easier de-excitation pathways and resultantly decrease fluorescence emission. Overall, the experimental EDD indicate that the decay plots are partly affected by the halogen's heavy-atom effect, providing a means to decreases emission by easier re-equilibration of the S_0 state. However, EDD and experimental QY suggest that other processes are at play for variations between **2** and **3**. To confirm this, theoretical calculations of the photochemical properties were performed, below.

Theoretical results

To review the QY variations for **1**, **2** and **3**, firstly the theoretical fluorescence plots were obtained alongside selected fluorescence properties, Figure 6 and Table 4.

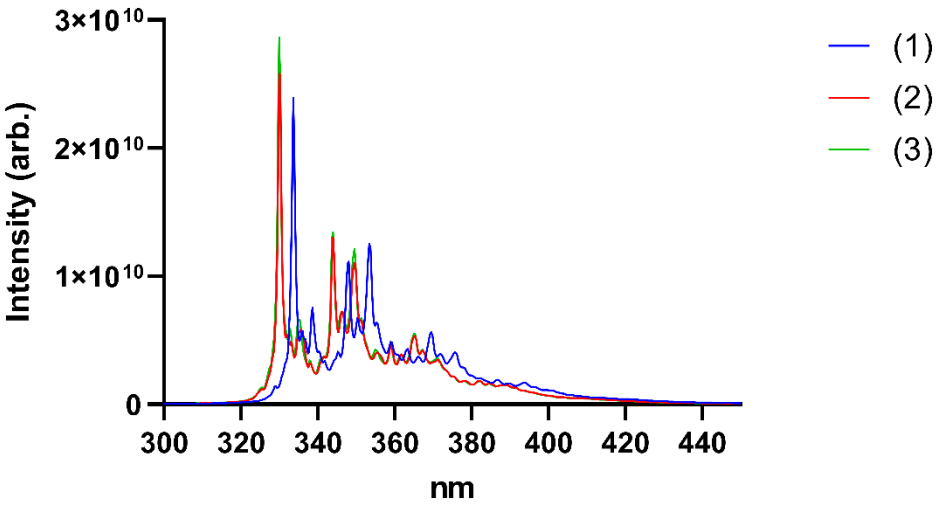

Figure 4. Theoretical fluorescence spectrums of **1**, **2**, and **3** were obtained using the ORCA_ESD module using a vertical gradient from S_1 to S_0, theory CAM-B3LYP/DEF2-TZVP in CPCM(water).

Table 4: Selected fluorescence properties from the ORCA_ESD calculations for **1**, **2** and **3**.

Compound	**Adiabatic Energy Difference** cm^{-1} / nm	**Fluorescence Rate Constant** (k_f) **(**s^{-1*}**)**	**τ (ns)**	Franck-Condon %	Herzberg-Teller %
1	29972 / 333	8.72 x 10^8	1.15	82.21	17.79
2	30295 / 330	8.49 x 10^8	1.18	80.57	19.43
3	30303 / 330	8.79 x 10^8	1.14	80.73	19.27

Figure 4, and Table 4 show the theoretical spin-orbit coupling free fluorescence plots and data for **1**, **2** and **3** based on the path integral approach.[45] Expectantly, this results in a poor estimate of the emission profiles. This is due to it following a singlet decay *via* the path integral approach with no mixing of the MOs.[45, 51] The results though do reflect that excitation of each compound is relatively equally in line with the experimental results (Figure S.6). To assess the halogen effect further, a set of calculations were performed to

obtain a comprehensive estimate of the Jablonski diagram. Here, the Jablonski is limited to rate constants which are derivable using DFT. This approach, include the ISC and phosphoresces profile of each compound. Using this method, it was shown that moving from fluoro- to iodo- there is a linear-$\log_{10}$ relationship between the level of SOC and the number of electron shells, this can further be expanded to the weights of the halide family (ESI, S.Figure 8). The results of SOC calculations indicate that fluorophores **2** and **3** may lose the remainder of the QY due to SOC contamination in the decay process.[9] This has been seen previously in the detection of halides by exploiting collisional quenching and SOC interactions.[17, 52, 68] This would result in the S_1 energy being dissipated through a forbidden transition to a T_x state. Here, the $T_{1,2,3}$ states were obtained allowing for deduction of the potential ISC rates (k_{isc}), as per Equation 2. the results of which can be found in Table 5. Lastly the, phosphoresces, Tx $\rightarrow S_0$, k_p, for all sub-spin states, was obtained using Equation 3. Combining the computational results the decay constants of k_f, k_{isc} and k_p for all compounds allow calculation of the QY using Equation 4.

Table 5: Theoretical radiative and nonradiative rates for **1**, **2** and **3** obtained using the path integral approach using ORCA_ESD.

compound	(k_f) (s^{-1*})	(k_{isc}) (s^{-1*}) (S_1 -> $T_{1,2,3}$)	(k_p) (s^{-1*})	Φ_{TE}
1	8.72 x 10^8	2.43 x 10^8	3.58	0.78
2	8.49 x 10^8	5.99 x 10^8	8.57	0.59
3	8.79 x 10^8	4.81 x 10^9	71.33	0.15

From Table 5 the loss of fluorescence in **3** is most prominent, the theoretical results overestimate the loss by 15% for **3**. However, considering this computational approach is limited and does not calculating the "full" Jablonski diagram (collision, re-excitation *etc*) the overestimation of QY loss is rather reasonable. This method looks at a single molecules photochemical state and does not include reflect a molecular environment completely. Further, expansion of the computational accuracy or application of an expanded molecular system could improve the SOC matrix determination and improve the accuracy of the calculation. Overall, here it shows the QY loss for **3** is from a mixture SOC in the excited states and the Br induced charge separation effect on $S_1 \rightarrow S_0$ energy dissipation seen in the EDD. For **2**, the ISC potential and resultant SOC is a magnitude lower compared to **3** and points at the Cl atom creating a charge separation as major reason for QY loss. Whilst the free-form **1** is well predicted 0.70 *vs*. 0.78, for experimental and theoretical, due to the lack of heavy atom effects. Here the theoretical prediction followed the experimental QY trend on a simple scaffold, this approach needs to be implemented on other scaffolds with varied complexity, R-group type, and solvent system before routine use.

Conclusions

In this work, a study of a series of halogenated 7-hydroxycoumarin fluorophores was performed. The combined use of charge density X-Ray diffraction and computational methods allowed for deconvolution of the experimental photoluminescence data. The fluorescence data showed that halogenation of the ortho position gave rise to decreased fluorescence QY. It was confirmed that **1**, **2** and **3** excited equally, this was confirmed using experimentally obtained EDDs of the ground state. The charge density HOMA and topology of **1**, **2**, and **3**, reflected this, however, the ESP maps and dipole moments showed that **2** to **3**

allows for a faster S_1 to S_0 re-equilibrium rate with excitation energy lost. This was assessed using theoretical fluorescence spectra obtained using TD-DFT and the path integral approach, the results did not discriminate the experimental results due only following a single excited state decay process. To gain information on the heavy-atom effect from Cl and Br, the SOC potentials were theoretically obtained. It was found that moving from F → Br → I lead to an exponential increase in SOC. The SOCs effect on fluorescence was explored with a new method based on *k* summations from the ISC and phosphorescence rates. This approach allowed for the rationalization of the experimental data, and it was shown that **3** had the largest ISC leading to a large decrease in QY, which paired with the dipole moment in the EDD creates a system that can dissipate the excitation energy well but lowers it QY. This approach also deemed that for **2** the major cause of QY loss was from the charge separation of S_0 as it had a relatively similar ISC potential as **1**, meaning that the small QY loss seen by Cl addition mainly affects charge re-equilibration. This approach was found to follow the experimental trends and be within reasonable error (max. 15%). Future studies are required to further validate the approach, with calculations on other flouro-probe scaffolds with experimental comparisons. It is hope that this information stimulate potential a probe designing platform following the trends seen in other aspect of chemical design.

References

1. Ejaz, M.; Mansha, A.; Asim, S.; Shahzad, A., Review article on "effects of ions on the fluorescence of coumarin derivatives". *Chem. pap*. **2022,** *76* (3), 1295-1311.
2. Tang, X.; Zhu, Z.; Liu, R.; Ni, L.; Qiu, Y.; Han, J.; Wang, Y., A novel OFF-ON-OFF fluorescence probe based on coumarin for Al3+ and F− detection and bioimaging in living cells. *Spectrochim Acta A Mol Biomol Spectrosc* **2019,** *211*, 299-305.
3. Ibrahim, H.; Caudron, E.; Kasselouri, A.; Prognon, P., Interest of Fluorescence Derivatization and Fluorescence Probe Assisted Post-column Detection of Phospholipids: A Short Review. *Mol.* **2010,** *15* (1), 352-373.
4. Matsuoka, Y.; Yamato, M.; Yamada, K.-i., Fluorescence probe for the convenient and sensitive detection of ascorbic acid. *J Clin Biochem Nutr* **2016,** *advpub*.

5. Kinoshita, M.; Negishi, M.; Sakai, H.; Hirano, T.; Mori, S.; Fujii, S.; Kagechika, H.; Tanatani, A., Development of 6-arylcoumarins as nonsteroidal progesterone antagonists. Structure–activity relationships and fluorescence properties. *Bioinorg. Chem* 2016**,** *24* (21), 5602-5610.
6. Fares, M.; Wu, X.; McNaughton, D. A.; Gilchrist, A. M.; Lewis, W.; Keller, P. A.; Arias-Betancur, A.; Fontova, P.; Pérez-Tomás, R.; Gale, P. A., A potent fluorescent transmembrane HCl transporter perturbs cellular pH and promotes cancer cell death. *Bioinorg. Chem* **2023,** *21* (12), 2509-2515.
7. Geddes, C. D., Optical halide sensing using fluorescence quenching: theory, simulations and applications-a review. *Meas. Sci. Technol.* **2001,** *12* (9), R53.
8. Xie, Y.; Yan, L.; Li, J., An On–Off–On Fluorescence Probe Based on Coumarin for Cu2+, Cysteine, and Histidine Detections. *Appl. Spectrosc.* **2019,** *73* (7), 794-800.
9. Valeur, B.; Berberan-Santos, M. N., *Molecular fluorescence: principles and applications*. John Wiley & Sons: 2012.
10. Du, J. J.; Váradi, L.; Tan, J.; Zhao, Y.; Groundwater, P. W.; Platts, J. A.; Hibbs, D. E., Experimental and theoretical charge density distribution in Pigment Yellow 101. *Phys Chem Chem Phys* **2015,** *17* (6), 4677-4686.
11. Váradi, L.; Hibbs, D. E.; Orenga, S.; Babolat, M.; Perry, J. D.; Groundwater, P. W., β-Alanyl aminopeptidase-activated fluorogenic probes for the rapid identification of Pseudomonas aeruginosa in clinical samples. *RSC Adv***.** **2016,** *6* (64), 58884-58889.
12. Raucci, U.; Chiariello, M. G.; Rega, N., Modeling excited-state proton transfer to solvent: A dynamics study of a super photoacid with a hybrid implicit/explicit solvent model. *J. Chem. Theory Comput.* **2020,** *16* (11), 7033-7043.
13. Gibson, J.; Monkman, A. P.; Penfold, T. J., The Importance of Vibronic Coupling for Efficient Reverse Intersystem Crossing in Thermally Activated Delayed Fluorescence Molecules. *ChemPhysChem* **2016,** *17* (19), 2956-2961.
14. Uejima, M.; Sato, T.; Tanaka, K.; Kaji, H., Enhancement of fluorescence in anthracene by chlorination: Vibronic coupling and transition dipole moment density analysis. *Chem. Phys.* **2014,** *430*, 47-55.
15. Wang, M.; Wang, X.; Li, X.; Yang, Z.; Guo, Z.; Zhang, J.; Ma, J.; Wei, C., A coumarin-fused 'off-on'fluorescent probe for highly selective detection of hydrazine. *Spectrochim Acta A Mol Biomol Spectrosc.* **2020,** *230*, 118075.
16. Aigner, D.; Freunberger, S. A.; Wilkening, M.; Saf, R.; Borisov, S. M.; Klimant, I., Enhancing photoinduced electron transfer efficiency of fluorescent pH-probes with halogenated phenols. *Anal. Chem.* **2014,** *86* (18), 9293-9300.
17. Misawa, R.; Matsuhashi, C.; Yamaji, M.; Mutai, T.; Yoshikawa, I.; Houjou, H.; Noguchi, K.; Maki, S.; Hirano, T., Halogen-substituent effect on the spectroscopic properties of 2-phenyl-6-dimethylaminobenzothiazoles. *Tetrahedron Lett.* **2019,** *60* (26), 1702-1705.
18. Chang, Y.; Hawkins, B. A.; Du, J. J.; Groundwater, P. W.; Hibbs, D. E.; Lai, F., A Guide to In Silico Drug Design. *Pharmaceutics* **2023,** *15* (1), 49.
19. Toutounji, M., A deeper look into Herzberg-Teller vibronic coupling effect and spectroscopic signature of non-Condon systems. *Chem. Phys.* **2019,** *523*, 205-210.
20. Lai, F.; Du, J. J.; Williams, P. A.; Váradi, L.; Baker, D.; Groundwater, P. W.; Overgaard, J.; Platts, J. A.; Hibbs, D. E., A comparison of the experimental and theoretical charge density distributions in two polymorphic modifications of piroxicam. *Phys Chem Chem Phys* **2016,** *18* (41), 28802-28818.
21. Hawkins, B. A.; Han, J.; Du, J. J.; Lai, F.; Stanton, S. A.; Divakarla, S. S.; Groundwater, P. W.; Platts, J. A.; Hibbs, D. E., Analyzing Hydration Differences in Cocrystal Polymorphs: High-Resolution X-ray Investigation of Caffeine–Glutaric Acid Cocrystals. *Cryst. Growth Des* **2021,** *21* (8), 4456-4467.
22. Stanton, S. A.; Du, J. J.; Lai, F.; Stanton, G.; Hawkins, B. A.; Ong, J. A.; Groundwater, P. W.; Platts, J. A.; Hibbs, D. E., Understanding Hygroscopicity of Theophylline via a Novel Cocrystal Polymorph: A Charge Density Study. *J. Phys. Chem. A* **2021,** *125* (45), 9736-9756.

23. Dubey, R.; Pavan, M. S.; Guru Row, T. N.; Desiraju, G. R., Crystal landscape in the orcinol:4,4'-bipyridine system: synthon modularity, polymorphism and transferability of multipole charge density parameters. *IUCrJ* **2014,** *1* (1), 8-18.
24. Waller, M. P.; Howard, S. T.; Platts, J. A.; Piltz, R. O.; Willock, D. J.; Hibbs, D. E., Novel properties from experimental charge densities: an application to the Zwitterionic neurotransmitter taurine. *Chem. - Eur. J.* **2006,** *12* (29), 7603-7614.
25. Du, J. J.; Stanton, S. A.; Fakih, S.; Hawkins, B. A.; Williams, P. A.; Groundwater, P. W.; Overgaard, J.; Platts, J. A.; Hibbs, D. E., Exploring the solubility of the carbamazepine-saccharin co-crystal; a charge density study. *Cryst. Growth Des* **2018**.
26. Srinivasa Gopalan, R.; Kumaradhas, P.; Kulkarni, G. U.; Rao, C. N. R., An experimental charge density study of aliphatic dicarboxylic acids. *Journal of Molecular Structure* **2000,** *521* (1), 97-106.
27. Hibbs, D. E.; Hanrahan, J. R.; Hursthouse, M. B.; Knight, D. W.; Overgaard, J.; Turner, P.; Piltz, R. O.; Waller, M. P., Experimental and theoretical charge distribution in (Z)-N-methyl-C-phenylnitrone. *Org. Biomol. Chem.* **2003,** *1* (6), 1034-1040.
28. Schmidtmann, M.; Farrugia, L. J.; Middlemiss, D. S.; Gutmann, M. J.; McIntyre, G. J.; Wilson, C. C., Experimental and Theoretical Charge Density Study of Polymorphic Isonicotinamide−Oxalic Acid Molecular Complexes with Strong O···H···N Hydrogen Bonds. *The J. Phys. Chem. A* **2009,** *113* (50), 13985-13997.
29. Nguyen, T. H.; Groundwater, P. W.; Platts, J. A.; Hibbs, D. E., Experimental and Theoretical Charge Density Studies of 8-Hydroxyquinoline Cocrystallized with Salicylic Acid. *J. Phys. Chem. A* **2012,** *116* (13), 3420-3427.
30. Nguyen, T. H.; Howard, S. T.; Hanrahan, J. R.; Groundwater, P. W.; Platts, J. A.; Hibbs, D. E., Experimental and Theoretical Charge Density Distribution in a Host-Guest System: Synthetic Terephthaloyl Receptor Complexed to Adipic Acid. *J. Phys. Chem. A* **2012,** *116* (23), 5618-5628.
31. Sovago, I.; Gutmann, M. J.; Senn, H. M.; Thomas, L. H.; Wilson, C. C.; Farrugia, L. J., Electron density, disorder and polymorphism: high-resolution diffraction studies of the highly polymorphic neuralgic drug carbamazepine. *Acta Crystallogr. B.* **2016,** *72* (1), 39-50.
32. Hoser, A. A.; Jarzembska, K. N.; Dobrzycki, Ł.; Gutmann, M. J.; Woźniak, K., Differences in Charge Density Distribution and Stability of Two Polymorphs of Benzidine Dihydrochloride. *Cryst. Growth Des* **2012,** *12* (7), 3526-3539.
33. Du, J. J.; Váradi, L.; Williams, P. A.; Groundwater, P. W.; Overgaard, J.; Platts, J. A.; Hibbs, D. E., An analysis of the experimental and theoretical charge density distributions of the piroxicam–saccharin co-crystal and its constituents. *RSC advances* **2016,** *6* (85), 81578-81590.
34. Hawkins, B. A.; Najib, E.; Du, J. J.; Lai, F.; Platts, J. A.; Groundwater, P. W.; Hibbs, D. E., Exploring the excited-state charge transfer fluorescence profile of 7-hydroxycoumarin and 2-methylimidazole – a combined X-ray diffraction and theoretical approach. *Phys Chem Chem Phys* **2022,** *24* (21), 13015-13025.
35. Chen, R. F., Fluorescent pH Indicator. Spectral Changes of 4-Methylumbelliferone. *Anal. Lett.* **1968,** *1* (7), 423-428.
36. Volkov, A.; Macchi, P.; Farrugia, L. J.; Gatti, C.; Mallinson, P.; Richter, T.; Koritsanszky, T. *XD2006- a computer program for multipole refinement, topological analysis of charge densities and evaluation of intermolecular energies from experimental or theoretical structure factors*, 2006.
37. Milnor, J. W., *Morse theory*. Princeton university press: 1963.
38. Neese, F.; Wennmohs, F.; Becker, U.; Riplinger, C., The ORCA quantum chemistry program package. *J. Chem. Phys.* **2020,** *152* (22), 224108.
39. Yanai, T.; Tew, D. P.; Handy, N. C., A new hybrid exchange–correlation functional using the Coulomb-attenuating method (CAM-B3LYP). *Chem. Phys. Lett.* **2004,** *393* (1), 51-57.
40. Tawada, Y.; Tsuneda, T.; Yanagisawa, S.; Yanai, T.; Hirao, K., A long-range-corrected time-dependent density functional theory. *J. Chem. Phys.* **2004,** *120* (18), 8425-8433.
41. Mitin, A. V.; Baker, J.; Pulay, P., An improved 6-31 G* basis set for first-row transition metals. *J. Chem. Phys.* **2003,** *118* (17), 7775-7782.

42. Koritsanszky, T. S.; Coppens, P., Chemical applications of x-ray charge-density analysis. *Chem. Rev. (Washington, D. C.)* **2001,** *101* (6), 1583-1627.
43. Keith, T. A. *AIMAll*, 14.06.21; TK Gristmill Software: Overland Park KS, USA, 2014.
44. Bader, R. F. W., *Atoms in Molecules: A Quantum Theory*. Oxford Univ. Press: 1994; p 454 pp.
45. de Souza, B.; Neese, F.; Izsák, R., On the theoretical prediction of fluorescence rates from first principles using the path integral approach. *J. Chem. Phys* **2018,** *148* (3), 034104-034104.
46. Weigend, F.; Ahlrichs, R, Balanced basis sets of split valence, triple zeta valence and quadruple zeta valence quality for H to Rn: Design and assessment of accuracy. *Phys Chem Chem Phys* **2005,** *7* (18), 3297-3305.
47. Becke, A. D., Density-functional thermochemistry. V. Systematic optimization of exchange-correlation functionals. *J. Chem. Phys* **1997,** *107* (20), 8554-8560.
48. Pantazis, D. A.; Chen, X.-Y.; Landis, C. R.; Neese, F., All-Electron Scalar Relativistic Basis Sets for Third-Row Transition Metal Atoms. *J. Chem. Theory Comput.* **2008,** *4* (6), 908-919.
49. Allen, F. H.; Kennard, O.; Watson, D. G.; Brammer, L.; Orpen, A. G.; Taylor, R., Tables of bond lengths determined by x-ray and neutron diffraction. Part 1. Bond lengths in organic compounds. *J. Chem. Soc., Perkin Trans. 2* **1987,** (12), S1-S19.
50. Caspar, J. V.; Meyer, T. J., Application of the energy gap law to nonradiative, excited-state decay. *J. Chem. Theory Comput.* **1983,** *87* (6), 952-957.
51. de Souza, B.; Farias, G.; Neese, F.; Izsák, R., Predicting Phosphorescence Rates of Light Organic Molecules Using Time-Dependent Density Functional Theory and the Path Integral Approach to Dynamics. *J. Chem. Theory Comput.* **2019,** *15* (3), 1896-1904.
52. Shi, L.; Liu, H.-Y.; Shen, H.; Hu, J.; Zhang, G.-L.; Wang, H.; Ji, L.-N.; Chang, C.-K.; Jiang, H.-F., Fluorescence properties of halogenated mono-hydroxyl corroles: the heavy-atom effects. *J Porphyr Phthalocya* **2009,** *13* (12), 1221-1226.
53. Gross, K. C.; Seybold, P. G., Substituent effects on the physical properties and pKa of phenol. *Int. J. Quantum Chem* **2001,** *85* (4-5), 569-579.
54. Lyssenko, K. A.; Grintselev-Knyazev, G. V.; Antipin, M. Y., Nature of the PO bond in diphenylphosphonic acid: experimental charge density and electron localization function analysis. *Mendeleev Commu* **2002,** *12* (4), 128-130.
55. Munshi, P.; Jelsch, C.; Hathwar, V. R.; Guru Row, T. N., Experimental and Theoretical Charge Density Analysis of Polymorphic Structures: The Case of Coumarin 314 Dye. *Cryst. Growth Des* **2010,** *10* (4), 1516-1526.
56. Du, J. J.; Stanton, S. A.; Fakih, S.; Hawkins, B. A.; Williams, P. A.; Groundwater, P. W.; Overgaard, J.; Platts, J. A.; Hibbs, D. E., Exploring the Solubility of the Carbamazepine–Saccharin Cocrystal: A Charge Density Study. *Cryst. Growth Des* **2018,** *21* (8), 4259-4275.
57. Borgoo, A.; Tozer, D. J.; Geerlings, P.; De Proft, F., Confinement effects on excitation energies and regioselectivity as probed by the Fukui function and the molecular electrostatic potential. *Phys Chem Chem Phys* **2009,** *11* (16), 2862-2868.
58. Madjet, M. E.; Abdurahman, A.; Renger, T., Intermolecular Coulomb Couplings from Ab Initio Electrostatic Potentials: Application to Optical Transitions of Strongly Coupled Pigments in Photosynthetic Antennae and Reaction Centers. *J. Phys. Chem. B* **2006,** *110* (34), 17268-17281.
59. Tsirelson, V.; Stash, A., Developing orbital-free quantum crystallography: the local potentials and associated partial charge densities. *Acta Crystallogr. B Struct. Sci. Cryst. Eng. Mater.* **2021,** *77* (4).
60. Tsirelson, V.; Stash, A., Orbital-free quantum crystallography: view on forces in crystals. Acta Crystallogr. B Struct. Sci. Cryst. Eng. Mater. **2020,** *76* (5), 769-778.
61. Zhang, M.; Yang, D.; Ren, B.; Wang, D., A TDDFT study on the excited-state intramolecular proton transfer (ESIPT): excited-state equilibrium induced by electron density swing. *J. Fluoresc.* **2013,** *23*, 761-766.
62. Krauss, M.; Jensen, J. O.; Hameka, H. F., Electronic structure of the excited states and phenol fluorescence. *J. Phys. Chem* **1994,** *98* (40), 9955-9959.

63. Alaminsky, R. J.; Seminario, J. M., Sigma-holes from iso-molecular electrostatic potential surfaces. *J. Mol. Model.* **2019,** *25* (6), 160.
64. Galande, C.; Mohite, A. D.; Naumov, A. V.; Gao, W.; Ci, L.; Ajayan, A.; Gao, H.; Srivastava, A.; Weisman, R. B.; Ajayan, P. M., Quasi-molecular fluorescence from graphene oxide. *Sci. Rep.***2011,** *1* (1), 85.
65. Smith, D. W., Effects of exchange energy and spin-orbit coupling on bond energies. *J. Chem. Educ.* **2004,** *81* (6), 886.
66. Rosokha, S. V.; Vinakos, M. K., Halogen bond-assisted electron transfer reactions of aliphatic bromosubstituted electrophiles. *Phys Chem Chem Phys* **2014,** *16* (5), 1809-1813.
67. Krygowski, T. M., Crystallographic studies of inter-and intramolecular interactions reflected in aromatic character of. pi.-electron systems. *J Chem Inf Comput Sci* **1993,** *33* (1), 70-78.
68. Lee, Y.; Malamakal, R. M.; Chenoweth, D. M.; Anna, J. M., Halogen bonding facilitates intersystem crossing in iodo-BODIPY chromophores. *J. Phys. Chem. Lett.* **2020,** *11* (3), 877-884.